Photomagnetic Carbon Nanotubes at Ambient Conditions

Wei Shen Lin[a], *Yueh-Hua Han*[a], *Ting-Yu Chang*[a], *Chong Mou Wang*[a]*,

Cheng-Hsun-Tony Chang[b] *and Jyh-Shen Tsay*[b]*

[a]Department of Chemistry and [b]Department of Physics, National Taiwan Normal University, Taipei 116, Taiwan

$Ru(bpy)_2(phen\text{-}NH_2)^{2+}$ was synthesized by reacting ruthenium(II) dichloride ($Ru(bpy)_2.2Cl$) with 5-amino-1,10-phenanthroline ($phen\text{-}NH_2$) in a hot ethanol-water mixture. Figure S1 shows its X-ray structure. According to the structure, $Ru(bpy)_2(phen\text{-}NH_2)^{2+}$ can be regarded as a structural analogue of $Ru(bpy)_3^{2+}$. The transient emission spectra associated with the excited $Ru(bpy)_2(phen\text{-}NH_2)^{2+}$ in water are presented in Figures S2. The lifetimes and quantum yields of the excited state in water, CH_2Cl_2 and CH_3CN are listed in Table S1 for comparison.

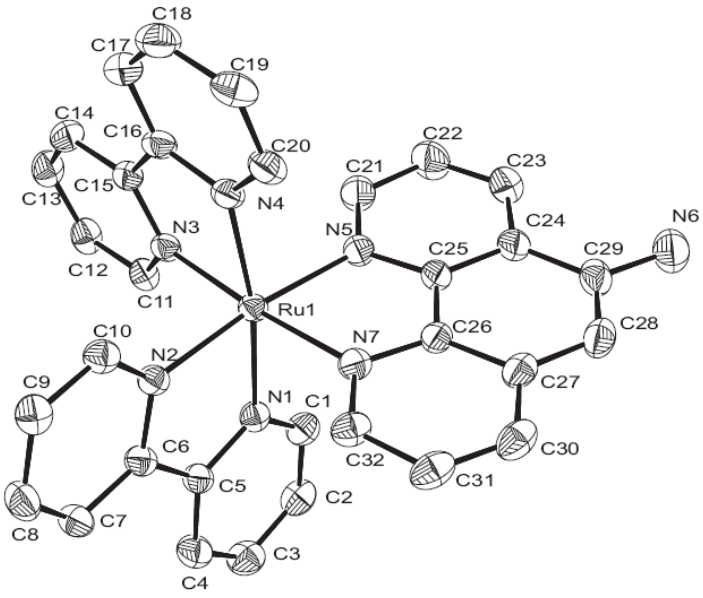

Figure S1. ORTEP view of the molecular structure of $Ru(bpy)_2(phen\text{-}NH_2)^{2+}$ with thermal ellipsoids shown at the 50% probability level.

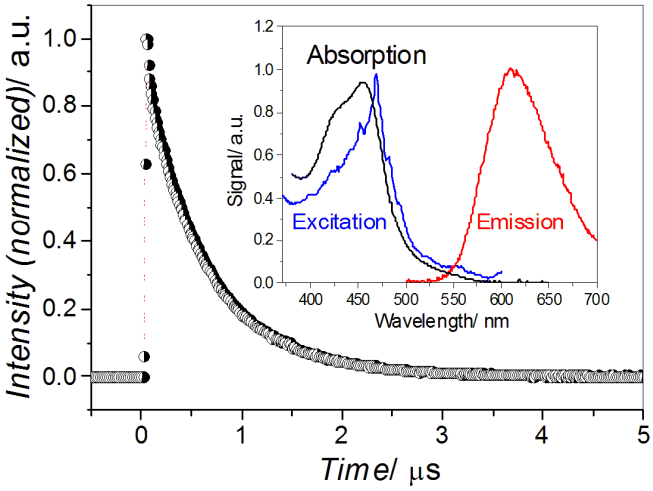

Figure S2. Transient emission spectra of the excited $Ru(bpy)_2(phen\text{-}NH_2)^{2+}$ recorded in water (λ_{ex}:473 nm; λ_{em}: 620 nm). Inset shows the associated excitation, absorption and emission spectra.

Table S1. Photophysical properties associated with the excited $Ru(bpy)_2(phen\text{-}NH_2)^{2+}$ and $Ru(bpy)_3^{2+}$ in various media.

Solvent	τ/ns [a]	Φ [a]	τ/ns [b]	Φ [b]
CH_2Cl_2	844	0.043	569	0.029
CH_3CN	933	0.068	850	0.062
H_2O	615	0.045	577	0.042

[a] $[Ru(bpy)_2(phen\text{-}NH_2)]^{2+}$; [b] $[Ru(bpy)_3]^{2+}$

When $Ru(bpy)_2(phen\text{-}NH_2)^{2+}$ reacted with carbon nanotubes (CNTs) in an acidic $NaNO_2$ solution, submicrodots were formed on the tubes. Figure S3 shows the TEM images of the resulting CNTs taken at various periods during the reaction. The $Ru(bpy)_2(phen\text{-}NH_2)^{2+}$-derived radicals formed small seeds on the CNT host at the early stage, and gradually transformed into beads with an average size of 100 nm after reaction for 1 h, and grew to be ~500 nm after 4 h. Figure S4 shows the representative UV-Vis absorption spectra of the Ru@CNT. The spectra of bare CNTs and $Ru(bpy)_2(phen\text{-}NH_2)^{2+}$ were also incorporated for comparison.

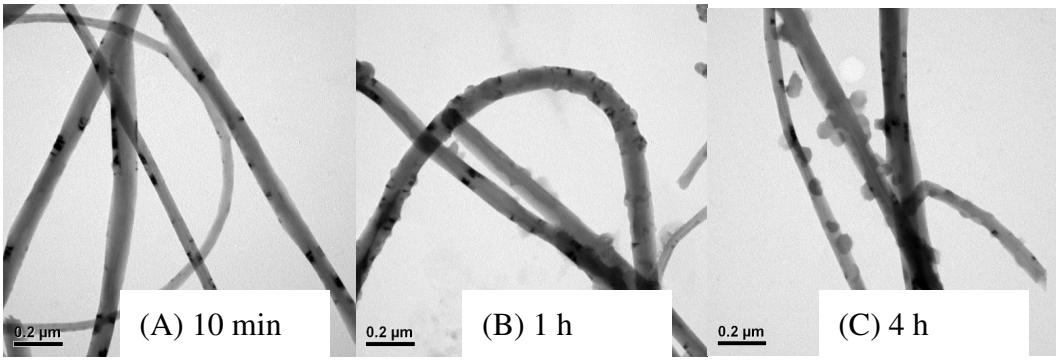

Figure S3. TEM images of CNTs taken at various periods during the reaction with $Ru(bpy)_2(phen\text{-}NH_2)^{2+}$ in an acidic $NaNO_2$ solution.

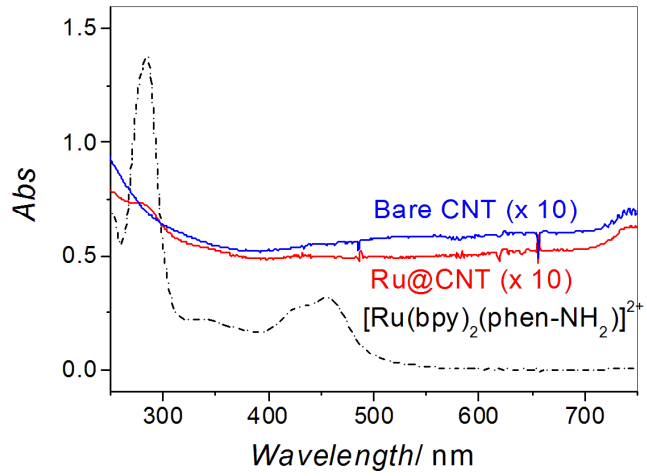

Figure S4. UV-Vis absorption spectra of $Ru(bpy)_2(phen\text{-}NH_2)^{2+}$, the Ru@CNT and bare CNTs.

We analyzed the conductivity of the bare CNTs and the Ru@CNTs by positioning them between two ITO glass electrodes (20 Ω/square), as shown in Figure S5.

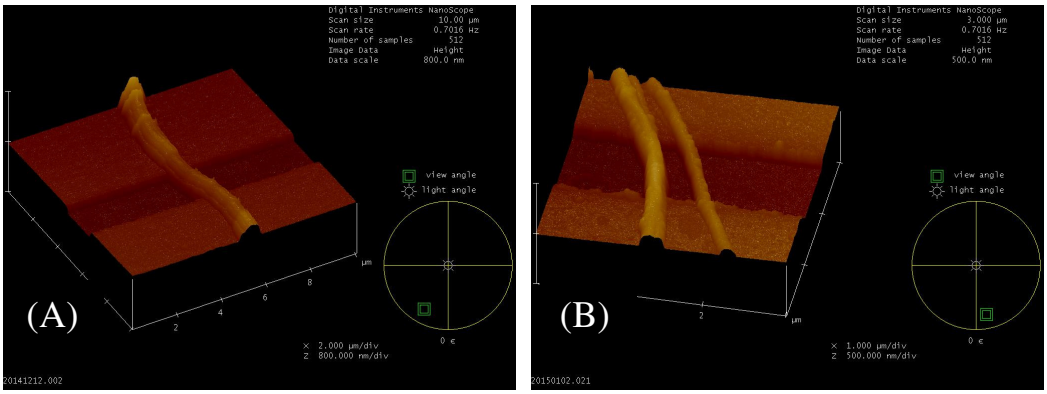

Figure S5. AFM images of one and two Ru@CNT tubes as positioned across a dielectric groove between two ITO electrodes during conductivity measurements.

$Ru(bpy)_2(phen\text{-}NH_2)^{2+}$ can also form nanodots on graphite (highly oriented pyrolyzed graphite, HOPG). Figure S6 shows the AFM images of a piece of HOPG before and after reacting with $Ru(bpy)_2(phen\text{-}NH_2)^{2+}$ under a condition similar to that for the Ru@CNTs. The resulting nanoparticles, ~50 nm in diameter, are uniformly deposited on the surface of the substrate, supporting the mechanism proposed in Scheme 1.

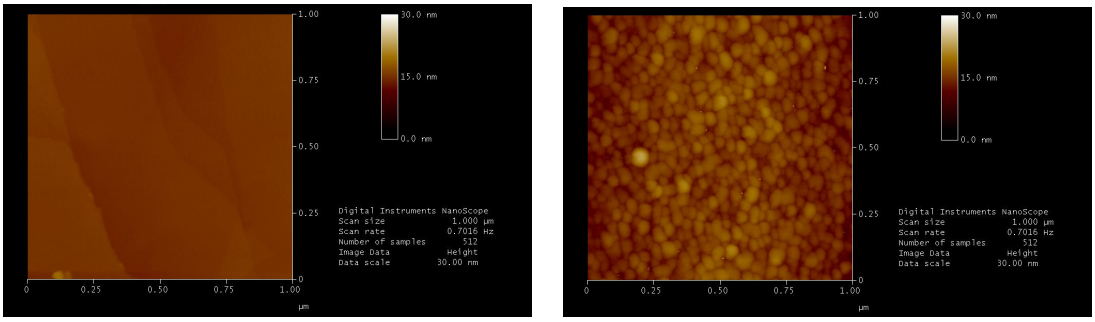

Figure S6. AFM images of a piece of HOPG before (left) and after (right) being modified with $Ru(bpy)_2(phen\text{-}NH_2)^{2+}$ in an acidic $NaNO_2$ solution.

We characterized the energetics of the Ru@CNT based on the excitation spectra (Figure S2) and the CV curves (Figure S7) of $Ru(bpy)_2(phen\text{-}NH_2)^{2+}$ under the assumption that $Ru(bpy)_2(phen\text{-}NH_2)^{2+}$ and Ru(II)-phen^{2+} share similar energetics. The 0-0 transition energy ($E_{0\text{-}0}$) for Ru(II)-phen^{2+} was estimated to be 2.27 eV, and the formal potentials of Ru(II)-phen$^{2+*/3+}$ and Ru(II)-phen$^{2+*/+}$, to be -1.0 and 1.0 V vs. SCE, respectively.

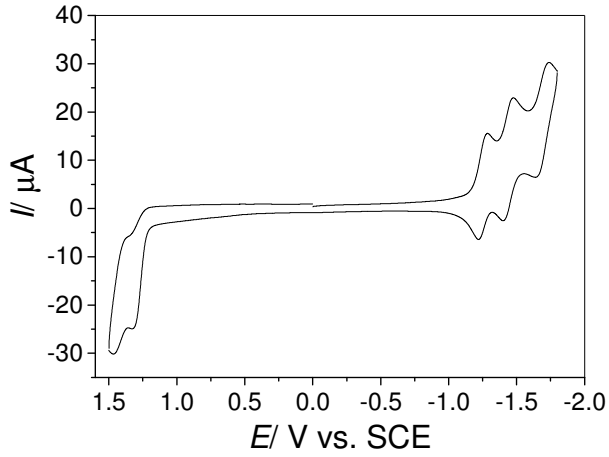

Figure S7. Representative CV curves of $Ru(bpy)_2(phen\text{-}NH_2)^{2+}$ (1 mM in 0.1 M $TBAPF_6/CH_3CN$, scan rate: 50 mV/s). The potential was calibrated with a silver pseudoreference electrode using ferrocene (Fc/Fc^+: 0.307 V vs. SCE) as the internal standard.

The phase shift caused by the nanodots depended on the power of the 473-nm light when the bias voltage was kept constant (V_b = 3 V), as shown in Figure S8. Since the

areas free of nanodots showed no appreciable effects on the same tip, we concluded that the power dependence was resulting from charge separation and not from a thermal effect induced by the incident light.

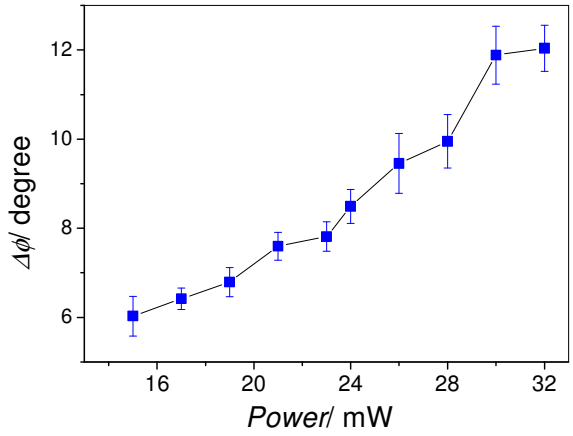

Figure S8. Correlation between $\Delta\phi$ and the power of the incident light (473 nm, V_b = 3 V).